Theoretical Investigation of Luminescence Behavior as a Function of Alkyl Chain Size in 4-Aminobenzonitrile Alicyclic Derivatives

Isabel Gómez, Yannick Mercier, and Mar Reguero*

Departament de Química i Inorgánica, Universitat Rovira i Virgili, C. Marcellí Domingo s/n, Tarragona 43007, Spain

Received: May 12, 2006; In Final Form: July 5, 2006

There is still controversy about the structure of the intramolecular charge transfer (ICT) emitting species in π-electron donor−acceptor systems that show dual fluorescence. Although the twisted ICT model is quite generally accepted, the planar ICT model is not ruled out because firm experimental evidence supports it. Among these it is the fact that some rigidized systems such as bicyclic 4-aminobenzonitrile derivatives exhibit dual fluorescence. We present here an ab initio CASSCF/CASPT2 study of a series of these compounds with the alicyclic chain ranging from 5 to 7 carbon atoms and compare their ICT mechanism with the more flexible 4-aminobenzonitrile (ABN) and 4-(dimethylamino)benzonitrile (DMABN). We present the energetics, geometries, and valence bond structures of the critical points of the potential-energy surfaces of the ground, local excited (LE), and ICT states. Our results show that the photophysical differences of the studied systems may be rationalized by two factors: the position of the ICT and LE potential-energy surfaces at the first stages of the ICT reaction and the relative energies of the excited-state minima. Computational evidence is presented that a twisted ICT structure can be adopted in some molecules such as NXC6 and NXC7 and that the anomalous band of the fluorescence spectra of these systems is emitted from a twisted ICT species.

Introduction

Intramolecular charge transfer (ICT) states in π-electron donor−acceptor systems have been the subject of considerable interest during the past four decades. Since its discovery by Lippert, 4-(dimethylamino)benzonitrile (DMABN), which exhibits dual fluorescence in polar solvents, has been the best-known prototype of such systems.[1] The nonlinear optical properties of these compounds have also given rise to intensive research in the field of organic materials because it is possible to use them as electrooptical switches, chemical sensors, and fluorescence probes.[2−4] Recently, some donor−acceptor systems have been used in the fabrication of molecular switches because of their dual fluorescence.[5] In these systems, absorption to the charge transfer (CT) $L_a(S_2)$ state is followed by ultrafast relaxation to the locally excited (LE) $L_b(S_1)$ state. Dual fluorescence then occurs from both the S_1 LE state (L_b-like minimum) and the S_1 (L_a-like) ICT minimum (for a review, see ref 6). The mechanism behind this phenomenon and the structure of the ICT-emitting species have been under debate for a long time.

Four different types of molecular structures have been proposed for the ICT-emitting species of DMABN. The most postulated model is the twisted ICT (TICT) model proposed by Grabowski[7,8] and supported by Rettig et al.[9−11] in which the amino group is perpendicular to the benzene ring. A planar ICT (PICT) model, in which the amino group lies in the benzene plane, has been suggested by Zachariasse for several years.[12−25] Two alternatives are the wagged ICT (WICT) model,[13,14,26] which involves a rehybridization from planar sp^2 to pyramidal sp^3 of the amino nitrogen, and the rehybridized ICT (RICT) model,[27−29] which involves a rehybridization of the cyano carbon from sp to sp^2 entailing a bent cyano bond. However, these last two models have little support these days.

Very recently, we reported the results of CASSCF, RASSCF, and CASPT2 calculations of 4-aminobenzonitrile (ABN) and DMABN.[30] From the three different ICT minima located, TICT, PICT, and RICT, we found that the twisted ICT (TICT) was the most stable in both molecules and located on the S_1 surface. The mechanism we propose to explain the dual fluorescence in these molecules is remarkably simple. After excitation to the S_2 (CT) state, the system quickly relaxes to a shallow S_2−PICT minimum from which it easily decays through a near conical intersection (CI) where the $S_2 \rightarrow S_1$ internal conversion takes place. In fact, the S_2/S_1 CT−LE radiationless decay can occur at any point on a extended conical intersection "seam" that runs almost parallel to the amino torsional coordinate. The lowest energy point on this conical intersection seam corresponds to a pyramidal structure in which the amino group is untwisted, so the branching at the CI favors formation of the LE state (the gradient of the lower surface leads to the LE minimum on the S_1 surface); however, the seam is accessible for a wide range of torsional angles, so if the decay takes place at large torsional angles, the probability of forming the S_1−TICT species is greater (here the gradient of the lower surface would lead to the TICT minimum on the S_1 surface). The two emitting S_1 species are also adiabatically linked along the amino torsion reaction coordinate. Thus, the S_1 LE−TICT equilibration and dual fluorescence will be controlled by (a) the position along the amino group twist coordinate where the S_2/S_1 CT−LE radiationless decay occurs and (b) the adiabatic S_1 torsional reaction path. For DMABN, LE and TICT can be populated because the stabilities of the two species are similar. However, in ABN, the equilibrium favors LE as a TICT state was found at much higher energy with a low reaction barrier toward LE and the minimum energy point of the CI has a pyramidal and untwisted

* To whom correspondence should be addressed. E-mail: mar.reguero@urv.net.

10.1021/jp062926k CCC: $33.50
Published on Web 09/19/2006

CHART 1: Structures of the Systems of the Series Studied

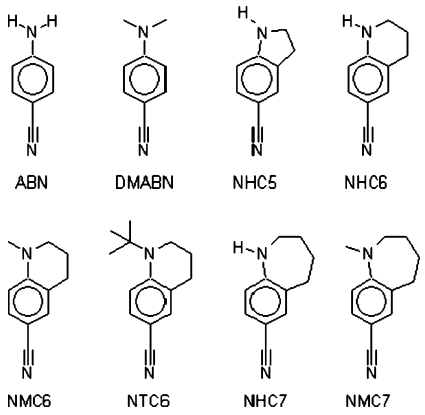

geometry. These characteristics of the potential-energy surfaces (PES) of the low-lying excited states explain why dual fluorescence cannot be observed in ABN.

There is still controversy, however, about whether the molecular structure of the ICT-emitting species in other π-electron donor−acceptor systems is twisted or planar. The main reasons why in recent years the TICT model has been the most postulated explanation of the ICT mechanism are the experimental observation of only the ICT fluorescence band in systems with a twisted ground-state equilibrium geometry (for example, in 3,5-dimethyl-4-(dimethylamino)benzonitrile[14]), even in nonpolar solvents, and the absence of ICT fluorescence in the emission spectra of such rigidized systems as 1-methyl-5-cyanoindoline (NMC5),[17,31] 1-methyl-6-cyano-1,2,3,4-tetrahydroquinoline (NMC6),[17,32] and 1-ethyl-5-cyanoindoline (NEC5),[12] even in strongly polar solvents such as acetonitrile or methanol. However, when the aliphatic ring becomes more flexible, as in the case of 1-methyl-7-cyano-2,3,4,5-tetrahydro-1*H*-1-benzazepine (NMC7),[16,17] fast and efficient ICT emission is observed both in polar and nonpolar solvents. Furthermore, a recent density functional theory study performed by Jamorski et al.[33,34] demonstrates that NMC7 is already twisted in its ground-state geometry, around 60°. These authors, therefore, suggest that only the twisted ICT model can explain the fluorescence characteristics of this kind of compounds since the high rigidity of the cycle in NMC5 and NMC6 prevents the TICT structure from forming whereas it forms easily in the more flexible NMC7.

Nevertheless, not long ago Zachariasse et al. again proposed the PICT model because they observed fast and efficient ICT emission in 1-*tert*-butyl-6-cyano-1,2,3,4-tetrahydroquinoline (NTC6)[25] in all solvents investigated, from nonpolar *n*-hexane to polar acetonitrile or methanol. They suggested that the ICT-emitting species is planar in NXC5 and NXC6 because the torsion of the amino group is sterically hindered. They also suggested that the different luminescence behavior in these systems is attributable to a different order of magnitude of the initial energy gap between the two excited states, $\Delta E(S_1,S_2)$, in the Franck−Condon region. For NTC6 this energy gap must be small and allow vibronic coupling, while for NMC6 and NMC5 the ΔE must be large. On the other hand, Köhn and Hättig[35] suggest that NTC6 may still be able to twist in its ICT state and that data in ref 25 do not necessarily exclude a TICT mechanism.

None of these hypotheses are inconsistent with the mechanism we propose for ICT.[30] Because pyramidalization is not constrained in these systems, the S_2/S_1 conical intersection will still be accessible along this coordinate. Although we found the ICT-emitting species to be the S_1−TICT state in the case of DMABN, we believe that the ICT S_1 minimum structure will depend on the system (type of compounds and substituents) and the environment (crystal or solution, polar or nonpolar solvent). We saw that it was necessary to investigate the potential-energy surfaces of such alicyclic systems to check if the anomalous emission can be attributed to a planar ICT structure and understand the effects of the substituents, which were sometimes very strong (as in the case of the replacement of methyl by *tert*-butyl groups). In this paper, we report the results of ab initio calculations at the CASSCF/CASPT2 level in 5-cyanoindoline (NHC5), 6-cyano-1,2,3,4-tetrahydroquinoline (NHC6), NMC6, NTC6, 7-cyano-2,3,4,5-tetrahydro-1*H*-1-benzazepine (NHC7), and NMC7 (see Chart 1). For the sake of comparison, the more flexible ABN and DMABN systems are also included. We will show that the topology of the potential-energy surfaces in NXC6 and NXC7 do not change in comparison with their more flexible counterparts ABN and DMABN since NXC6 and NXC7 are able to twist. Actually, the energy gap between the two initial excited states, $\Delta E(S_1,S_2)$, and the energetics of the LE and ICT minima are key to explaining the different luminescence behavior of the systems studied. In particular, these factors will explain why only NTC6 and NMC7 out of the series show dual fluorescence in polar and nonpolar solvents.

Computational Details

The different electronic states of ABN, DMABN, NHC5, NHC6, NMC6, NTC6, NHC7, and NMC7 have been studied with the complete active space self-consistent field (CASSCF)[36] method using a 6-31G(d) basis set.[37] The 12 electrons and 11 orbitals that constitute the active space include the benzene π and π^* orbitals, the amino nitrogen lone pair, and the four π and π^* orbitals of the cyano group. Full geometry optimizations were performed without any symmetry constraint. Numerical frequency calculations were carried out to determine the nature of the stationary points. Intrinsic reaction coordinates (IRCs)[38] were also computed to determine the pathways linking the critical structures (stationary points and CI).

Conical intersections were optimized using the algorithm described in ref 39. State averaged orbitals were used, and the orbital rotation derivative correction (which is usually small) to the gradient was not computed. This gives the lowest energy point on the crossing at which there are two coordinates, the gradient difference and derivative coupling vectors (branching space), which lift the degeneracy. The remaining $3N - 8$ coordinates (intersection space) preserve the degeneracy, which therefore persists over a wide range of molecular geometries. Depending on the kinetic energy of the system, decay can take place away from the minimum energy point on the crossing.

To incorporate the effect of the dynamic valence-electron correlation on the relative energies of the lower excited states, we made second-order multiconfigurational perturbation theory calculations based on the CASSCF(12,11) reference function (CASPT2).[40] CASPT2 single-point energies were calculated at the CASSCF (12,11)/6-31G(d) optimized geometries and performed using an average of states between the three lowest energy singlet states $S_0/S_1/S_2$. Nevertheless, in some zones of the potential-energy surfaces where the S_1 and S_2 states were almost degenerate and very high with respect to the ground state, an average 0.5/0.5 between the S_1/S_2 states was used. This is the case for the S_2/S_1 conical intersection. All CASPT2 computations were performed using the completed Fock matrix to define the zero-order Hamiltonian together with an imaginary level shift of 0.2 to prevent incorporation of intruder states.[41]

The CAS state interaction method (CASSI)[42] was used to compute the transition dipole moments of the various excited states in the Franck−Condon region, which were then used together with the excitation energies to determine the values of the oscillator strength.

Valence bond (VB) structures were determined using the results of the computation of the second-order exchange density matrix P_{ij} and the diagonal elements of the electronic density matrix (see ref 43 for details). The elements of P_{ij} have a simple physical interpretation, which is related to the spin coupling between the electrons localized in the orbitals residing on the atoms i and j.[44] An illustration of the meaning of these matrix elements can be found in ref 43.

The CASSCF calculations were carried out with the Gaussian 03 system of programs,[45] whereas the CASSI and CASPT2 computations were performed with the MOLCAS 6.0 program package.[46]

Results and Discussion

A. Geometry and VB Structures of the Ground-State, LE, and ICT Minima. We shall start by discussing the geometry of the various critical points located and describing the wave functions in terms of VB language. Actually, the structural and electronic descriptions of the various minima are at the heart of the TICT controversy.

First, we located (at the CASSCF level) the various minima on the S_0, S_1, and S_2 PES of NHC5, NXC6, and NXC7 that correspond to the ground-state, LE, TICT, and PICT stable species. As in ABN and DMABN,[30] we found a planar ICT stable species lying on the S_2 potential-energy surface but could not locate a S_1−PICT minimum. Twisted ICT minima were located on the S_1 surface of every compound of the series studied except for NHC5, which cannot adopt this structure because of its greater rigidity. The S_1−RICT minima, too high in energy in ABN and DMABN to be mechanistically interesting, were not looked for. The geometries of the minima located are shown in Figure 1 together with the VB structures derived from the analysis of the corresponding wave function (from the values of the second-order exchange density matrixes and the one−electron matrixes which are shown in Figure S1 of the Supporting Information). Table 1 collects the values of the wagging angle (θ) and twist angle (φ) of the relaxed structures. The CASSCF/CASPT2 relative energies and the dipole moments of these relaxed structures are shown in Table S1.

These results show that the electronic structure of the ground-state minimum (S_0−GS) corresponds to an in-phase combination of the two Kekulé structures. It is clear that this covalent nature is retained in the S_1−LE state, with similar dipole moments but with an anti-Kekulé benzene moiety. The S_2−PICT and S_1−TICT minima have similar zwitterionic characters with a partial or net positive charge on the nitrogen atom of the amino group and a resonant quinoidal phenyl anion, giving rise to large dipole moments. The values of this property obtained here (see Table S1) are systematically lower than the experimental data because the latter were measured in polar solvents while the former were calculated in the gas phase. The major difference between S_2−PICT and S_1−TICT is the magnitude of the charge transfer (fraction of electron transferred), which, as expected, is slightly greater in TICT (see Figure S1). The values of the second−order exchange density matrixes collected in Figure S1 show that the coupling between the nitrogen lone pair and the phenyl ring is larger in the ICT structures, PICT and TICT, than in the more covalent ones, GS and LE.

Let us now discuss the relaxed geometries shown in Figure 1. The ground-state geometries of ABN and DMABN are untwisted with a pyramidal amino group.[30] The angle between the plane of the amino group and the phenyl ring (wagging angle, θ) is 43° and 26°, respectively. This geometric feature is retained in NHC5, NHC6, and NMC6 (see Table 1). However, NTC6, NHC7, and NMC7 possess somewhat twisted ground-state equilibrium geometries with twist angles of 33°, 38°, and 46°, respectively, and a practically nonpyramidal amino group (near sp^2 hybridization). This finding can be explained by the strong steric hindrance between the *tert*-butyl group, in NTC6, and the *o*-hydrogen in the phenyl ring. In NXC7, the conformation of the aliphatic ring imposes a pretwisted ground-state geometry rather than a planar one.

The optimized geometries for the S_1−LE minima closely resemble those of the ground state. Similar wagging and twist angles are found in the corresponding geometries (Table 1). The main difference is that the phenyl CC bonds in the excited state are expanded, as expected from the out-of-phase combination of two Kekulé structures.

One of the main arguments against the TICT model, in which the amino group is perpendicular to the benzene ring, is the general agreement that it can only be adopted by very flexible 4-aminobenzonitriles, like ABN and DMABN. Actually, in the five-membered ring compound NHC5 no TICT structure was located because of the restricted flexibility of the amino group, which was structurally fixed to be nearly coplanar to the ring. However, in the NXC6 systems the alkyl chain is long enough to allow a partial rotation of the amino group. Thus, we located twisted ICT minima in NHC6, NMC6, and NTC6 at 62°, 65°, and 69°, respectively. The more flexible the aliphatic ring is, the larger the twist angle, which reaches values of 82° and 85° in the TICT structures of NHC7 and NMC7, respectively. Our calculations show that, as in ABN and DMABN, these TICT species are slightly bent with the nitrogen of the amino group and the carbon of the phenyl ring taking the group out of the ring plane and in an anti position.

As in ABN and DMABN, the phenyl ring of all the S_1−TICT and S_2−PICT structures exhibits a quinoidal geometry: the two CC central bonds of the benzene ring are much shorter than the other four CC bonds. However, in the S_1−TICT structures, the $N-C_{phenyl}$ bond length is larger than in the ground-state one (almost single bond length) whereas in S_2−PICT the $N-C_{phenyl}$ bond is shorter (practically double bond length).

B. Excited States in the Franck−Condon Region. Table 2 shows the computed excitation energies of NHC5, NXC6, and NXC7 in the gas phase, together with the dipole moments and the oscillator strengths of the lowest excited states determined by CASSCF and CASPT2 calculations. The corresponding excitation energies of ABN and DMABN are also included for comparison. These energies were calculated as the vertical difference between the excited state and the ground-state energies, at the ground-state-optimized geometry.

No qualitative or quantitative differences are observed between these systems at the CASSCF level. The first excited state is the LE (L_b-like) one in all cases with very similar dipole moments of around 5−6 D. The oscillator strengths for this excitation are very small, indicating its weakly allowed character. The CT (L_a-like) state is the second excited state, characterized by a high dipole moment of around 12−14 D and a strong oscillator strength, which indicate that it should be considered as the initially promoted state. This state will carry most of the energy after absorption because of the allowed character of the transition. Though the CASSCF results agree qualitatively with the experimental data in nonpolar sol-

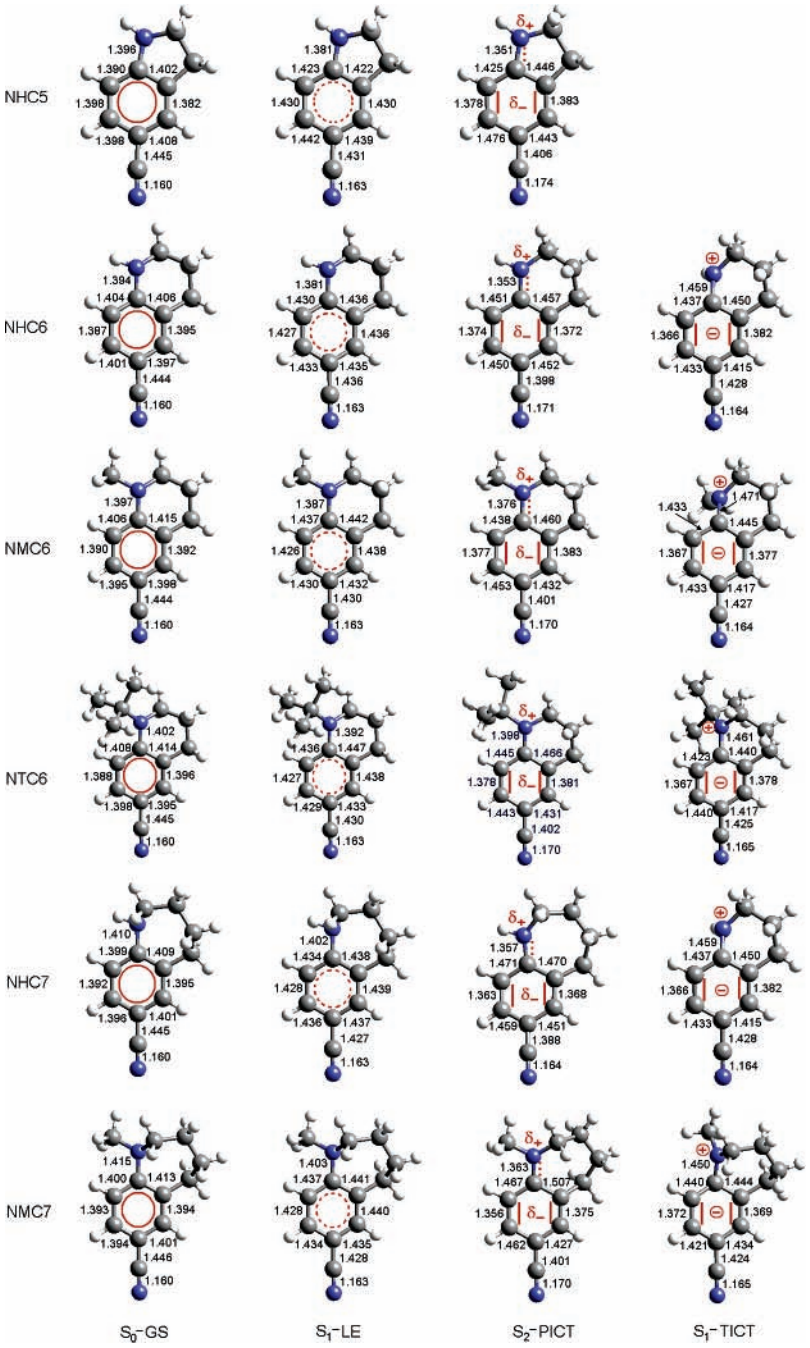

Figure 1. Geometries of the ground-state, LE, PICT, and TICT minima and VB structures of the different systems studied.

TABLE 1: Selected Geometrical Parameters of the Optimized Structures: Wagging Angle (θ) and Twist Angle (φ)

	ABN		DMABN		NHC5		NHC6		NMC6		NTC6		NHC7		NMC7	
structure[a]	θ	φ	θ	φ	θ	φ	θ	φ	θ	φ	θ	φ	θ	φ	θ	φ
S_0−GS	43	0	26	0	33	0	24	0	19	0	0	33	0	38	0	46
S_1−LE	40	0	21	0	31	0	20	0	19	0	0	35	0	36	0	44
S_1−TICT	0	90	0	90			0	62	0	65	0	69	0	82	0	85

[a] Note that all S_2−PICT species show $\theta = 0°$ and $\varphi = 0°$.

vents,[16,17,25,31,32] the energetics are highly overestimated, particularly for the CT state, where the disagreement is more than 30 kcal mol^{-1}. To obtain more accurate results, we recalculated the energies with the CASPT2 method to include the dynamic correlation.

As can be seen from the results shown in Table 2, the dynamic electron correlation has a different quantitative effect on the LE and CT states. For both states the CASPT2 excitation energies are smaller than the CASSCF ones, but the LE state undergoes a smaller stabilization of around 10 kcal mol^{-1}, whereas the CT state is stabilized by around 30 kcal mol^{-1}. These CASPT2 results are now in reasonable agreement with the available experimental data. It seems that dynamic electron correlation effects are of critical importance for obtaining quantitatively accurate results, especially in the computation of the excitation energies. A direct consequence of this discriminatory effect of the dynamic electron correlation is that the energy gap between the two excited states decreases. The variation of the CASPT2 energy difference between the LE and CT states throughout the series of compound studied is depicted in Figure 2a. The energy difference is smaller when the alkyl chain is larger (for example, $\Delta E(S_1,S_2)$ in ABN is more than twice the gap in DMABN), as the charge transfer state is stabilized in molecules with long, more polarizable chains attached to the

TABLE 2: Excitation Energies (kcal mol^{-1}), Dipole Moments (μ, in Debyes), and Oscillator Strengths (f) Obtained at the Franck−Condon Region in the Gas Phase for the Different Systems Studied[a]

molecule	state	ΔE CASSCF	ΔE CASPT2	exp	$\Delta E(S_1,S_2)$ CASPT2	μ	f
ABN	LE	111.0	101.9	>92[b]	16.2	5.3	0.068
	CT	152.0	118.1	>109[b]		11.8	0.478
DMABN	LE	111.0	99.1	92−102[c]	7.2	6.0	0.006
	CT	140.7	106.3	99−106[c]		13.8	0.608
NHC5	LE	110.5	99.1		11.3	5.3	0.063
	CT	146.1	110.4			14.5	0.399
NHC6	LE	109.9	98.4		11.3	5.7	0.006
	CT	144.6	109.7			12.8	0.500
NMC6	LE	109.9	97.2		6.7	5.9	0.006
	CT	139.3	103.9	99.5[d]		13.5	0.556
NTC6	LE	109.4	95.3		−0.7	6.1	0.005
	CT	137.9	94.6	95.7[d]		14.0	0.508
NHC7	LE	111.8	102.3		10.4	5.2	0.000
	CT	145.9	112.7			11.8	0.398
NMC7	LE	111.2	101.7		0.3	5.2	0.000
	CT	147.3	102.0	96.4[e]		13.8	0.388

[a] Experimental values of absorption energies are included for comparison. [b] Absorption energy in *n*-heptane (ref 14). [c] Absorption energy in the gas phase (ref 47). [d] Absorption energy in *n*-hexane (ref 25). [e] Absorption energy in *n*-hexane (ref 17).

nitrogen atom of the amino group. This effect is surprisingly strong for NTC6 and NMC7, where the CT state is degenerate with the LE. It should be pointed out that these are the only systems in the series that present anomalous fluorescence even in nonpolar solvents. Zachariasse suggested that the efficiency of the ICT reaction in *n*-hexane was much greater for NTC6 and NMC7 than for DMABN because of the decrease in the energy gap.[25] Our results seem to confirm this.

The fact that the energy of the CT state is almost degenerate with that of the LE state in the Franck−Condon region in NTC6 and NMC7 could be explained by (a) the geometry of the ground state in these systems and (b) the effect of the substituents in the amino group. As we have shown previously, the ground state in NTC6 and NMC7 displays a pretwisted geometry that favors the CT over the LE state because it is strongly stabilized by the twisting mode. Additionally, replacement of methyl by *tert*-butyl (NMC6/NTC6) or of hydrogen by methyl (NHC7/NMC7) enhances ICT efficiency because the charge generated by the electron transfer is delocalized by the interaction between the amino nitrogen lone pair orbital and the molecular orbitals of the alkyl substituents. This assumption was also made by Serrano-Andrés et al.[48] in an extensive theoretical study on DMABN, where the main component of the reaction pathway was assumed to involve an amino group twist.

C. Mechanistic Overview. The luminescent characteristics of the π-electron donor−acceptor systems studied here will be determined by the relative energies and the connection between the potential-energy surfaces of the low-lying excited states LE and ICT. From a mechanistic point of view, it is the potential surface topology that is important and the energetics do not need to be highly accurate to provide qualitative mechanistic information. In this case though the effect of the dynamic correlation is so different on both states that it can qualitatively change the interplay between the states, so it must be included in the ab initio calculations. Accordingly, we used the CASPT2 method to recalculate the energies of the critical points located at the CASSCF level for the NHC5, NXC6, and NXC7 systems discussed in section A. CASPT2 calculations have also been run for the DMABN for comparative purposes.

The LE minima of all the molecules of the series studied (including ABN and DMABN) lie on the S_1 surface (S_1−LE). For the ICT, the planar minimum was found to be always on the S_2 surface (S_2−PICT) while the twisted one was always located on the S_1 surface (S_1−TICT). It is worth noting that although at the CASPT2 level some of the PICT species are more stable than the TICT ones, the emission will never take place from the second excited-state potential-energy surface, so the PICT species cannot be an emitting one.

Two elements force the geometry of the ICT species and determine their relative energies. First, let us consider the restricted flexibility of the aliphatic ring. The shorter the alkyl chain is, the more difficult it is for a stable TICT structure to form to such an extent that this structure has not been located for NHC5. The population of the LE and PICT minima, therefore, is favored for compounds with short alkyl chains. Second, we must take into account the steric hindrance between the substituents of the amino group and the *o*-hydrogen in the phenyl ring. This hindrance enforces pretwisted geometries for the ground-state and LE species, destabilizing them relative to the TICT species. In fact, in those systems with a pretwisted ground-state structure (NTC6, NHC7, and NTC7) the high energy of the PICT species (that is, higher than the energy of the TICT structure) indicates that the planar geometry is very unfavorable. On the other hand, in systems with a planar ground state (i.e., ABN, NHC6, and NMC6) the PICT structure is more stable than the TICT structure, although the former lies on the S_2 potential-energy surface and the latter on the S_1 one. These results can be seen in Figure 2b, which shows a diagram of the CASPT2 energies of the LE, PICT, and TICT structures for each system. Relative CASSCF and CASPT2 energies and dipole moments are collected in Table S1 of the Supporting Information.

Because the CT state is S_2 in the Franck−Condon region but S_1 in the TICT structure at the CASSCF level, the first part of the reaction path after light absorption must be nonadiabatic. That is, at this level of theory the S_1 and S_2 surfaces must cross. We located the lowest energy point on the S_1/S_2 conical intersection in these systems. Their energies are collected in Table S1. Because the geometry optimization of these critical points is carried out at the CASSCF level, when the energies are recalculated at the CASPT2 level it is found that the S_1 and S_2 states are no longer degenerate. Unfortunately, the commercial software available nowadays does not allow a better approximation. Figure S2 shows these structures together with the two degeneracy-lifting coordinates that define the branching space (the derivative coupling vector and the gradient difference vector) in all systems studied. The characteristics of the conical intersections found for NHC5, NHC6, NMC6, NTC6, NHC7, and NMC7 are the same as those reported for ABN and DMABN:[30] there is an extended seam that runs parallel to the $CN(Me)_2$ torsion coordinate. The branching space does not involve either the amino group twist or the pyramidalization coordinates; rather, it is dominated by skeletal deformations of the phenyl ring coupled with C−N stretch, so the S_1/S_2 degeneracy is preserved along the amino group torsion. Thus, $S_2 \rightarrow S_1$ internal conversion can take place at the full range of torsion angles depending on the vibrational energy in torsional coordinates following photoexcitation, but the highest probability corresponds to the minimum energy point of the seam. This structure has different twist and pyramidalization angles for the different alicyclic derivatives of the series, as will be discussed below. The deexcitation will be followed by an adiabatic equilibration between the LE- and ICT-emitting species on the S_1 potential-energy surface. The energy of the TS of this adiabatic path will be similar to that of the S_1/S_2 CI, as the TS

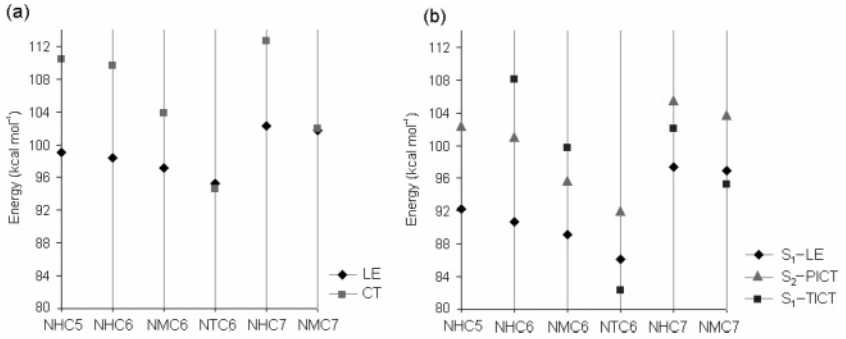

Figure 2. (a) Excitation energies of the LE and ICT states at the Franck−Condon region for the compounds of the series studied. (b) Energies of the LE, PICT, and TICT minima for the different systems studied relative to their corresponding ground-state minima.

is generated in the neighborhood of the CI due to the associated avoided crossing. For all systems the initial excitation energy is larger than the energy of the minimum of the CI seam, which means that the TS of the LE−ICT interconversion is always accessible. The luminescence behavior will also depend on the relative energy of the LE- and ICT-emitting species. As Figure 2b shows, the TICT structure is thermodynamically favored over the LE structures only for NTC6 and NMC7, which are the only structures capable of producing the anomalous fluorescence band in nonpolar solvents.

Our computational results show that the overall topology of the potential-energy surfaces of the LE and ICT states in these 4-aminobenzonitrile alicyclic derivatives do not change substantially in comparison with the ones of the more flexible ABN and DMABN. The energy corrections caused by including the dynamic electron correlation do not modify the relative positions of the LE and ICT states, and consequently, the mechanistic conclusions drawn in ref 30 still hold. Thus, the S_1 LE−TICT equilibration and dual fluorescence will be controlled by (a) the position along the amino group twist coordinate where the S_2/S_1 CT−LE internal conversion takes place and (b) the S_1 adiabatic reaction path between the LE and TICT minima. Taking this into account we can distinguish several types of systems. For ABN, NHC5, NHC6, NMC6, and NHC7, the amino group is untwisted at the lowest point of the S_2/S_1 conical intersection seam, so the branching at the CI favors formation of the LE state. Moreover, the S_1−LE species are much more stable than the S_1−TICT ones (see Figure 2b and Table S1), so the equilibrium will favor the LE species. This explains why, in these molecules, ICT emission cannot be observed in the fluorescence spectra. Note that in NHC5 the S_2/S_1 conical intersection will lead directly to the S_1−LE structure since this system cannot adopt any other stable structure on the S_1 potential-energy surface.

However, at the lowest energy point of the S_1/S_2 conical intersection located at the CASSCF level for NTC6 and NMC7, the amino group is slightly twisted (21.2° and 31.9°, respectively), so branching at the CI favors formation of the TICT state. If only CASPT2 results are taken into account, the energy gap between the two excited states in the Franck−Condon region is small enough to allow vibronic coupling between the CT and LE states, so both minima would be populated simultaneously. The adiabatic S_1 reaction path connecting them will displace the equilibrium toward the TICT minimum because it is less energetic. Consequently, observation of dual fluorescence emission in nonpolar solvents is in very good agreement with our results. It is worth pointing out that the LE and CT states are degenerate in the Franck−Condon region only for NTC6 and NMC7. This, together with the fact that the stability of the TICT species is greater than that of the LE species, is key to explaining the ICT emission of these molecules in nonpolar solvents. These characteristics are clearly reflected in Figure 2. A polar solvent will stabilize the ICT state even further, so in this case the initial excitation will populate the CT state that will correspond to the first excited state. The system will relax over the S_1 surface directly to the S_1 minimum, the TICT-emitting species, without undergoing any internal conversion. This direct mechanism explains why the ICT reaction is much more efficient in these systems than in DMABN in polar solvents.

The DMABN is a halfway case. The geometry of the minimum energy point of the S_1/S_2 conical intersection minimum is a pyramidal untwisted structure, but the LE and TICT minima are almost degenerate in the gas phase. This is in good agreement with its luminescent behavior, which presents only the LE normal band in nonpolar solvents and dual fluorescence in polar ones, where the TICT minimum will be stabilized further than the LE one.

Conclusions

According to our results, two factors rationalize the photophysical differences between the systems studied. First, the position of the TICT and LE potential-energy surfaces in the first stages of the ICT reaction must be considered. If the CT state is higher in energy than the LE in the Franck−Condon region and the lowest energy point on the CI is located at a planar geometry, the LE minimum will be populated first. On the other hand, if the CI lowest energy point has a twisted geometry or the CT state is lower in energy than the LE in the Franck−Condon region, the TICT minimum will be populated first.

In the next stage of the reaction the second factor plays its role. The relative energies of the LE and TICT minima will determine the displacement of the equilibrium between the two species along the adiabatic path that connects them over the S_1 surface. The minimum that is not reached in the first stages of the reaction can now be populated if it is more stable than the other one. This factor is strongly sensitive to the presence of polar solvents that will preferentially stabilize the CT state.

Thus, our conclusions agree partially with Zachariasse's generalization that relates the efficiency of the ICT process to the energy gap between the S_1 and S_2 states in the Franck−Condon region.[25] On the other hand, and in contrast to Zachariasse's hypothesis, our results suggest that the ICT species responsible for the anomalous fluorescence band in the NTC6 and NMC7 spectra must have a twisted structure. We present computational evidence that a twisted ICT structure can very well be adopted by these bicyclic but still slightly flexible molecules. A full perpendicular twist of the amino group is not

necessary to get a stable ICT structure on the S_1 surface when the alkyl chain is long enough. Therefore, the experimental results in ref 25 do not necessarily exclude a TICT fluorescence emission.

Nevertheless, it is possible that in other systems structural or environmental changes (in the donor or acceptor moieties with the addition of further substituents and/or the inclusion of solvent effects) could modify the relative energies of the key structures or their location. This, in turn, can modify the outcome of the CT reaction and change the fluorescence behavior in different compounds. In particular, the PICT structure can stabilize to such an extent that it becomes a first excited-state structure. In this case, it could be a radiative species of the anomalous fluorescence band in competition with the TICT species. This qualitative modification of the interplay between the LE and ICT surfaces would explain why there is so much contradictory evidence in favor of the TICT and PICT models. As a result, it is not advisable to propose a general mechanism for the CT reaction, and each particular case must be studied in detail.

Acknowledgment. This work has been supported the Spanish Ministry of Education and Science (project no. CTQU2005-08459-C02-02/BQU) and the Generalitat de Catalunya (Ajuts per grups d′investigació reconeguts, grant 2005SGR-00104).

Supporting Information Available: Equilibrium geometries, electronic structures, VB structures, and relative energies at the CASSCF/CASPT2 level of the different minima located; geometries of the S_1/S_2–CI and branching space. This material is available free of charge via the Internet at http://pubs.acs.org.

References and Notes

(1) Lippert, E.; Lüder, W.; Boos, H. In *Advances in Molecular Spectroscopy*; Mangini, A., Ed.; Pergamon: Oxford, 1962; pp 443−457.

(2) Bosshard, C.; Sutter, K.; Pretre, P.; Hulliger, J.; Florsheimer, M.; Kaatz, P.; Gunter, P. *Organic Nonlinear Optical Materials*; Advances in Nonlinear Optics; Gordon and Breach Publishers: New York, 1995; Vol. 1.

(3) Kippelen, B.; Lackritz, H. S.; Claus, R. O. *Organic Nonlinear Optical Material and devices*; Materials Research Society: Warrendale, PA, 1999.

(4) Lakowicz, J. P. *Principles of Fluorescence Spectroscopy*, 2nd ed.; Kluwer Academic: Hongham, 1999.

(5) (a) La Clair, J. J. *Angew. Chem., Int. Ed. Engl.* **1999**, *38*, 3045. (b) La Clair, J. J. *Angew. Chem., Int. Ed. Engl.* **1998**, *37*, 325. (c) La Clair, J. J. *J. Am. Chem. Soc.* **1997**, *119*, 7676.

(6) Grabowski, Z. R.; Rotkiewicz, K.; Rettig, W. *Chem. Rev.* **2003**, *103*, 3899.

(7) Rotkiewicz, K.; Grellmann, K. H.; Grabowski, Z. R. *Chem. Phys. Lett.* **1973**, *19*, 315.

(8) Rotkiewicz, K.; Grellmann, K. H.; Grabowski, Z. R. *Chem. Phys. Lett.* **1973**, *21*, 212.

(9) Köhler, G.; Rechthaler, K.; Rotokiewicz, K.; Rettig, W. *Chem. Phys.* **1996**, *207*, 85.

(10) Gude, C. C.; Rettig, W. *J. Phys. Chem. A* **1998**, *102*, 7754.

(11) Rettig, W.; Lutze, S. *Chem. Phys. Lett.* **2001**, *341*, 263.

(12) Leinhos, U.; Kühnle, W.; Zachariasse, K. A. *J. Phys. Chem.* **1991**, *95*, 2013.

(13) Schuddeboom, W.; Jonker, S. A.; Warman, J. H.; Leinhos, U.; Kühnle, W.; Zachariasse, K. A. *J. Phys. Chem.* **1992**, *96*, 10809.

(14) Zachariasse, K. A.; von der Haar, T.; Hebecker, A.; Leinhos, U.; Kühnle, W. *Pure Appl. Chem.* **1993**, *65*, 1745.

(15) von der Haar, T.; Hebecker, A.; Il'ichev, Y. V.; Jiang, Y.-B.; Kühnle, W.; Zachariasse, K. A. *Recl. Trav. Chim. Pays−Bas* **1995**, *114*, 430.

(16) Zachariasse, K. A.; Grobys, M.; von der Haar, T.; Hebecker, A.; Il'ichev, Y. V.; Jiang, Y.-B.; Morawski, O.; Kühnle, W. *J. Photochem. Photobiol., A: Chem.* 1996, *102*, 59. Erratum: *J. Photochem. Photobiol., A: Chem.* **1998**, *115*, 259.

(17) Zachariasse, K. A.; Grobys, M.; Von der Haar, T.; Hebecker, A.; Il'ichev, Y. V.; Morawski, O.; Rückert, I.; Kühnle, W. *J. Photochem. Photobiol., A* **1997**, *105*, 373.

(18) Il'ichev, Y. V.; Kühnle, W.; Zachariasse, K. A. *J. Phys. Chem. A* **1998**, *102*, 5670.

(19) Chudoba, C.; Kummrow, A.; Dreyer, J.; Stenger, J.; Nibbering, E. T. J.; Elsaesser, T.; Zachariasse, K. A. *Chem. Phys. Lett.* **1999**, *309*, 357.

(20) Zachariasse, K. A. *Chem. Phys. Lett.* **2000**, *320*, 8.

(21) Demeter, A.; Druzhinin, S.; George, M.; Haselbach, E.; Roulin, J.-L.; Zachariasse, K. A. *Chem. Phys. Lett.* **2000**, *323*, 351.

(22) Daum, R.; Druzhinin, S.; Ernst, D.; Rupp, L.; Schroeder, J.; Zachariasse, K. A. *Chem. Phys. Lett.* **2001**, *341*, 272.

(23) Druzhinin, S. I.; Demeter, A.; Galievsky, V. A.; Yoshihara, T.; Zachariasse, K. A. *J. Phys. Chem. A* **2003**, *107*, 8075.

(24) Techert, S.; Zachariasse, K. A. *J. Am. Chem. Soc.* **2004**, *126*, 5593.

(25) Zachariasse, K. A.; Druzhinin, S. I.; Bosch, W.; Machinek, R. *J. Am. Chem. Soc.* **2004**, *126*, 1705.

(26) Gorse, A.-D.; Pesquer,. *J. Phys. Chem.* **1995**, *99*, 4039.

(27) Sobolewski, A. L.; Domcke, W. *Chem. Phys. Lett.* **1996**, *259*, 119.

(28) Sobolewski, A. L.; Domcke, W. *Chem. Phys. Lett.* **1996**, *250*, 428.

(29) Sobolewski, A. L.; Sudholt, W.; Domcke, W. *J. Phys. Chem. A* **1998**, *102*, 2716.

(30) Gómez, I.; Reguero, M.; Boggio-Pasqua, M.; Robb, M. A. *J. Am. Chem. Soc.* **2005**, *117*, 7119.

(31) Visser, R. J.; Varma, C. A. G. O. *J. Chem. Soc., Faraday Trans. 2* **1980**, *76*, 453.

(32) Rotkiewicz, K.; Grabowski, Z. R.; Krówczyñski, A.; Kühnle, W. *J. Lumin.* **1976**, *12/13*, 877.

(33) Jamorski Jödicke, C.; Lüthi, H. P. *J. Am. Chem. Soc.* **2003**, *125*, 252.

(34) Jamorski Jödicke, C.; Lüthi, H. P. *J. Chem. Phys.* **2003**, *24*, 12852.

(35) Köhn, A.; Hättig, C. *J. Am. Chem. Soc.* **2004**, *126*, 7399.

(36) For a review, see: Roos, B. O. *Adv. Chem. Phys.* **1987**, *69*, 399.

(37) (a) Herhe, W. J.; Ditchfield, R.; Pople, J. A. *J. Chem. Phys.* **1972**, *56*, 2257. (b) Harihan, P. C.; Pople, J. A. *Theor. Chim. Acta* **1973**, *28*, 213.

(38) (a) Fukui, K. *Acc. Chem. Res.* **1981**, *14*, 363. (b) Schmidt, M. W.; Gordon, M. S.; Dupuis, M. *J. Am. Chem. Soc.* **1985**, *107*, 2585. (c) Gonzalez, C.; Schlegel, B. *J. Chem. Phys.* **1989**, *90*, 2154. (d) Gonzalez, C.; Schlegel, B. *J. Phys. Chem.* **1990**, *94*, 5523.

(39) (a) Celani, P.; Robb, M. A.; Garavelli, M.; Bernardi, F.; Olivucci, M. *Chem. Phys. Lett.* **1995**, *243*, 1−8. (b) Garavelli, M.; Celani, P.; Fato, M.; Bearpark, M. J.; Smith, B. R.; Olivucci, M.; Robb, M. A. *J. Phys. Chem. A* **1997**, *101*, 2023.

(40) (a) Anderson, K.; Malmqvist, P.-A.; Roos, B. O.; Sadlej, A. J.; Wolinski, K. *J. Phys. Chem.* **1990**, *94*, 5483. (b) Anderson, K.; Malmqvist, P.-A.; Roos, B. O. *J. Chem. Phys.* **1992**, *96*, 1218.

(41) (a) Roos, B. O.; Andersson, K. *Chem. Phys. Lett.* **1995**, *245*, 215. (b) Roos, B. O.; Andersson, K.; Fülscher, M. P.; Serrano-Andrés, L.; Pierloot, K.; Merchán, M.; Molina, V. *J. Mol. Struct. Theochem* **1996**, *388*, 257.

(42) (a) Malmqvist, P.-Å. *Int. J. Quantum Chem.* **1986**, *30*, 479. (b) Malmqvist, P.-Å.; Roos, B. O. *Chem. Phys. Lett.* **1989**, *155*, 189.

(43) Blancafort, L.; Celani, P.; Bearpark, M. J.; Robb, M. A. *Theor. Chem. Acc.* **2003**, *110*, 92.

(44) McWeeny, R.; Sutcliffe, B. T. *Molecular Quantum Mechanics*; Academic Press: New York, 1969; pp 148−170.

(45) Frisch, M. J.; Trucks, G. W.; Schlegel, H. B.; Scuseria, G. E.; Robb, M. A.; Cheeseman, J. R.; Montgomery, J. A., Jr.; Vreven, T.; Kudin, K. N.; Burant, J. C.; Millam, J. M.; Iyengar, S. S.; Tomasi, J.; Barone, V.; Mennucci, B.; Cossi, M.; Scalmani, G.; Rega, N.; Petersson, G. A.; Nakatsuji, H.; Hada, M.; Ehara, M.; Toyota, K.; Fukuda, R.; Hasegawa, J.; Ishida, M.; Nakajima, T.; Honda, Y.; Kitao, O.; Nakai, H.; Klene, M.; Li, X.; Knox, J. E.; Hratchian, H. P.; Cross, J. B.; Bakken, V.; Adamo, C.; Jaramillo, J.; Gomperts, R.; Stratmann, R. E.; Yazyev, O.; Austin, A. J.; Cammi, R.; Pomelli, C.; Ochterski, J. W.; Ayala, P. Y.; Morokuma, K.; Voth, G. A.; Salvador, P.; Dannenberg, J. J.; Zakrzewski, V. G.; Dapprich, S.; Daniels, A. D.; Strain, M. C.; Farkas, O.; Malick, D. K.; Rabuck, A. D.; Raghavachari, K.; Foresman, J. B.; Ortiz, J. V.; Cui, Q.; Baboul, A. G.; Clifford, S.; Cioslowski, J.; Stefanov, B. B.; Liu, G.; Liashenko, A.; Piskorz, P.; Komaromi, I.; Martin, R. L.; Fox, D. J.; Keith, T.; Al-Laham, M. A.; Peng, C. Y.; Nanayakkara, A.; Challacombe, M.; Gill, P. M. W.; Johnson, B.; Chen, W.; Wong, M. W.; Gonzalez, C.; Pople, J. A. *Gaussian 03*, revision B.05; Gaussian, Inc.: Wallingford, CT, 2004.

(46) Andersson, K.; Barysz, M.; Bernhardsson, A.; Blomberg, M. R. A.; Cooper, D. L.; Fleig, T.; Fülscher, M. P.; DeGraaf, C.; Hess, B. A.; Karlström, G.; Lindh, R.; Malmqvist, P.-Å.; Neográ dy, P.; Olsen, J.; Roos, B. O.; Sadlej, A. J.; Schütz, M.; Schimmelpfennig, B.; Seijo, L.; Serrano-Andrés, L.; Siegbahn, P. E. M.; Stålring, J.; Thorsteinsson, T.; Veryazov, V.; Widmark, P.-O. *MOLCAS*, version 6.0; Department of Theoretical Chemistry, Lund University: Sweden, 2004.

(47) (a) Herbish, J.; Pérez-Salgado, F.; Rettschnick, R. P. H.; Grabowski, Z. R.; Wójtovicz, H. J. *J. Phys. Chem.* **1991**, *95*, 3491. (b) Bulliard, C.; Allan, M.; Wirt, G.; Haselbach, E.; Zachariase, K. A.; Detzer, N.; Grimme, S. *J. Phys. Chem. A* **1999**, *103*, 7766.

(48) Serrano-Andrés, L.; Merchán, M.; Roos, B. O.; Lindh, R. *J. Am. Chem. Soc.* **1995**, *117*, 3189.